



## Article

# Choline Oxidase-Incorporated ATRP-Based Cerium Nanogels as Nanozymes for Colorimetric Detection of Hydrogen Peroxide and Choline

Trung Hieu Vu <sup>1</sup>, Byung Jo Yu <sup>2,\*</sup> and Moon Il Kim <sup>1,\*</sup>

<sup>1</sup> Department of BioNano Technology, Gachon University, 1342 Seongnamdae-ro, Sujeong-gu, Seongnam 13120, Republic of Korea; hieu.vutrong24596@gmail.com

<sup>2</sup> Low-Carbon Transition R&D Department, Research Institute of Sustainable Development Technology, Korea Institute of Industrial Technology (KITECH), Cheonan 31056, Republic of Korea

\* Correspondence: bjyu@kitech.re.kr (B.J.Y.); moonil@gachon.ac.kr (M.I.K.)

**Abstract:** Choline is an important molecule in monitoring food safety and infant nutrition. Here, we report Ce nanogels synthesized by atom transfer radical polymerization (ATRP) employing Ce-coordinated acryloyl-lysine polymer brushes (Ce@SiO<sub>2</sub> NGs) as highly efficient cascade nanozymes for colorimetric detection of choline. The synthesized Ce@SiO<sub>2</sub> NGs demonstrated remarkable peroxidase-like activity with a porous exterior, which are essential to entrap choline oxidase (COx) to yield COx@Ce@SiO<sub>2</sub> NGs and construct a cascade reaction system to detect choline. Immobilized COx catalyzed the oxidation of choline in food samples to produce H<sub>2</sub>O<sub>2</sub>, which subsequently induced the oxidation of chromogenic substrate 3,3',5,5'-tetramethylbenzidine (TMB) to produce blue color signals. This method enabled the selective and sensitive detection of target choline with a satisfactory linear range of 4–400 μM, which is sufficient to analyze foodborne choline. The practical utility of the COx@Ce@SiO<sub>2</sub> NG-based assay was successfully validated to determine choline spiked in commercially available milk and infant formula with high accuracy and precision values. This approach provides a simple and affordable method of choline detection and has the potential to lead to more developments in ATRP-based nanozymes for diverse biosensing applications.

**Keywords:** ATRP-based nanogels; cascade reaction; peroxidase-like nanozymes; choline detection; food safety



**Citation:** Vu, T.H.; Yu, B.J.; Kim, M.I. Choline Oxidase-Incorporated ATRP-Based Cerium Nanogels as Nanozymes for Colorimetric Detection of Hydrogen Peroxide and Choline. *Biosensors* **2024**, *14*, 563. <https://doi.org/10.3390/bios14120563>

Received: 22 October 2024

Revised: 17 November 2024

Accepted: 20 November 2024

Published: 21 November 2024



**Copyright:** © 2024 by the authors. Licensee MDPI, Basel, Switzerland. This article is an open access article distributed under the terms and conditions of the Creative Commons Attribution (CC BY) license (<https://creativecommons.org/licenses/by/4.0/>).

## 1. Introduction

Choline is an essential nutrient for developing the brain and maintaining overall health [1–3]. Several diseases, such as Alzheimer’s disease, liver cirrhosis, and growth disorder, were suggested to be induced by long-term choline deficiency [4,5]. Usually, the body can restore choline through food intake, and, thus, accurate determination of choline in foods is an important issue. The US Food and Drug Administration (FDA) as well as the food and nutrition board (FNB) of the institute of medicine thus set regulations that infant formula not made from cow’s milk must be supplemented with a high choline concentration (up to 200 mg/100 g sample), which is equivalent to that of breast milk (~1 mM) [6]. In addition, H<sub>2</sub>O<sub>2</sub> is commonly used as a disinfectant in food preservation; however, its excessive levels can pose health risks, such as oxidative stress and tissue damage [7,8]. Therefore, ensuring accurate quantification of choline as well as H<sub>2</sub>O<sub>2</sub> in foods is essential for maintaining health standards and meeting dietary needs [6,9]. The traditional detection methods for choline and H<sub>2</sub>O<sub>2</sub>, such as high-performance liquid chromatography (HPLC) and fluorescence-based techniques, are generally selective and sensitive. However, these approaches present several challenges, including time-consuming sample pre-/post-treatment, interference from background signals, and the inevitable use of complicated instrumentation [7,10,11]. Thus, the development of more convenient,

reliable, and sensitive methods for detecting choline and residual  $H_2O_2$  is vital to overcome these limitations and improve food safety and nutritional assessments.

Recent advancements in nanotechnology have highlighted the potential of nanomaterials with enzyme-like properties, known as nanozymes, to replace natural enzymes in versatile applications. Nanozymes possess several superiorities to natural enzymes, such as enhanced stability and durability, tunable activity, and more affordable synthesis [12,13]. Despite these advantages, natural enzymes often outperform nanozymes in terms of substrate specificity and catalytic efficiency. This is primarily due to the intricate and finely tuned structure of the active sites in natural enzymes, which nanozymes struggle to replicate. To bridge this gap, recent studies have focused on designing more sophisticated nanozyme architectures, with attention on engineering their active sites. Notably, materials with metal–nitrogen (M–N) active sites, such as Fe–N, Co–N, Zn–N, or metal–organic frameworks (MOFs), have emerged as highly promising candidates [14–17]. M–N active site materials have mimicked the active centers of natural metalloenzymes, while MOFs provide nanoscale cavities resembling the three-dimensional (3D) binding pockets of natural enzymes, creating a conducive environment for the catalytic process. These advances in nanozyme development provide new opportunities in versatile applications from biochemical sensing and environmental remediation to medical theranostics [18].

Building on these developments, nanogels synthesized via ATRP have emerged as a promising platform for improving the catalytic performance of nanozymes. ATRP is recognized as a controlled polymerization method that enables the precise synthesis of well-defined, biocompatible nanogels. These nanogels are characterized by exceptional biocompatibility, tunable porosity, and the ability to create dynamic microenvironments around catalytic centers that resemble the active sites of natural enzymes [19–23]. Recently, an enzyme-catalyzed variant of this method, called ATRPase, was introduced. This approach enables the synthesis of biocompatible polymer brushes through the interfacial polymerization of amino-acid-based monomers, such as N-acryloyl-L-lysine. By coordinating with certain metal ions including Fe, these polymeric nanogels exhibited unique enzyme-like activities [24,25]. Although the potential of ATRP-based nanozymes has been demonstrated, further investigations are required to study the effects of versatile metal ions regarding incorporation within the nanogels to induce affirmative enzyme-like activity for their practical applications.

Cerium (Ce) ions exhibit exceptional qualities as effective cross-linkers in the formation of various hydrogel-based materials. Their integration into the hydrogel matrix through cross-linking enhances the structural stability and mechanical properties of the hydrogels while enabling the creation of materials with tailored functionalities [26–28]. By leveraging the unique coordination chemistry of Ce ions, researchers have designed hydrogels with affirmative properties, such as improved stability, increased loading capacities, and enhanced catalytic activities, making them suitable for diverse applications in the biomedical and environmental fields [29,30]. Moreover, the ability of Ce ions to alternate between  $Ce^{3+}$  and  $Ce^{4+}$  oxidation states promotes strong peroxidase-like activity, making them highly effective for various biosensing applications [14]. Additionally, the monoatomic dispersion of Ce ions within the hydrophilic network of the nanogels possibly creates a high density of active sites, resulting in significantly improved reaction rates and overall catalytic efficiency [31,32]. These advantageous properties position Ce-based nanogels as promising materials for advanced catalytic and biosensing platforms.

Herein, we developed Ce nanogels synthesized by ATRP employing Ce-coordinated acryloyl-lysine polymer brushes ( $Ce@SiO_2$  NGs) as an efficient peroxidase mimic and scaffold for oxidative enzyme entrapment, which is designed for colorimetric detection of  $H_2O_2$  and choline by incorporating COx within the nanogels. The Ce ions within the  $Ce@SiO_2$  NGs serve as both structural cross-linkers and active centers, leading to enhanced catalytic efficiency. Additionally, the ATRP-based nanogels provided a biocompatible and porous network that is capable of entrapping COx, resulting in  $COx@Ce@SiO_2$  NGs performing selective and sensitive choline detection via a cascade reaction. In the presence

of choline, COx catalyzed its oxidation to produce H<sub>2</sub>O<sub>2</sub>, which subsequently activated the peroxidase-mimicking Ce@SiO<sub>2</sub> NGs to oxidize a chromogenic substrate TMB to produce a blue color. This provides a dual-function platform capable of detecting choline as well as H<sub>2</sub>O<sub>2</sub>. By leveraging the catalytic properties of Ce@SiO<sub>2</sub> NGs and COx@Ce@SiO<sub>2</sub> NGs, a versatile, reliable, and scalable method has been developed to enhance food safety analysis, particularly in the context of dairy products and infant nutrition.

## 2. Materials and Methods

### 2.1. Reagents and Materials

2-Bromoisobutanoic acid N-hydroxysuccinimide ester (NHS-Bib), sodium hydroxide (NaOH), sodium carbonate (Na<sub>2</sub>CO<sub>3</sub>), sodium acetate (CH<sub>3</sub>COONa), sodium ascorbate, copper sulfate pentahydrate (CuSO<sub>4</sub>·5H<sub>2</sub>O), TMB, ammonia solution (28% in water), dimethyl sulfoxide (DMSO), tetraethyl orthosilicate (TEOS), cerium(III) nitrate hexahydrate (Ce(NO<sub>3</sub>)<sub>3</sub>·6H<sub>2</sub>O), absolute ethanol, acryloyl chloride, L-lysine hydrochloride, horseradish peroxidase (HRP), 3-aminopropyl triethoxysilane (APTES), phosphate buffered saline (PBS), and 8-hydroxyquinoline were purchased from Sigma-Aldrich (St. Louis, MO, USA). Hydrogen peroxide was obtained from Samchun Chemical (Seoul, Republic of Korea). All solutions were prepared with deionized (DI) water purified by a Milli-Q Purification System (Millipore, Darmstadt, Germany).

### 2.2. Material Characterizations

Using a Field Emission Scanning Electron Microscope (JSM-7500F JEOL, Pleasanton, CA, USA) for scanning electron microscopy (SEM) and a Transmission Electron Microscope (FEI Tecnai, Hillsboro, OR, USA) for transmission electron microscopy (TEM) and high-resolution TEM (HR-TEM), the morphology of the Ce@SiO<sub>2</sub> NGs was examined. Energy-dispersive spectroscopy (EDS) was used to analyze the elemental composition (Bruker, Billerica, MA, USA). The suspension of sonicated Ce@SiO<sub>2</sub> NGs was allowed to dry overnight on a silicon wafer in preparation for the SEM examinations. Further, 5 μL of the sonicated nanogel suspension was deposited onto a carbon-coated copper TEM grid (Electron Microscopy Sciences, Hatfield, PA, USA) for the TEM studies, and it was then allowed to dry overnight at room temperature (RT). An FT-IR spectrophotometer (FT/IR-4600, JASCO, Easton, MD, USA) was used to acquire the Fourier transform infrared (FT-IR) spectra of Ce@SiO<sub>2</sub> NGs. X-ray photoelectron spectroscopy (XPS) was conducted using an XPS reader (Sigma Probe, Thermo Scientific, Madison, WI, USA) to analyze the contribution of elements. Water contact angle was measured to investigate the hydrophilicity of Ce@SiO<sub>2</sub> NGs using a Phoenix 300 contact angle analyzer (Surface Electro Optics, Suwon, Gyeonggi, Republic of Korea).

### 2.3. Synthesis of Ce@SiO<sub>2</sub> NGs and Ce@SiO<sub>2</sub> NGs Entrapping COx (COx@Ce@SiO<sub>2</sub> NGs)

Ce@SiO<sub>2</sub> NGs were synthesized from SiO<sub>2</sub> nanoparticles (NPs), N-acryloyl-L-lysine brush, and Ce(NO<sub>3</sub>)<sub>2</sub> solution following reported method with minor modifications [24]. First, N-acryloyl-L-lysine solution (50 mg/mL), SiO<sub>2</sub>-Br NP dispersion (5 mg/mL), and sodium ascorbate solution (1.5 mg/mL) were mixed thoroughly in PBS (10 mM, pH 6) under nitrogen atmosphere. Next, HRP (5 mg/mL) as an ATRP catalyst (ATRPase) was added and the solution was oscillated overnight at RT. In order to obtain the nanogel layer at the surface of nanoparticles, Ce(NO<sub>3</sub>)<sub>3</sub>·6H<sub>2</sub>O was added to the solution and stirred for 2 h at RT to induce the cross-linking process of lysine moieties at the surface of polymer brushes (N-acryloyl-L-lysine). The Ce-coordinated nanogel on SiO<sub>2</sub> surfaces (Ce@SiO<sub>2</sub> NGs) was obtained by centrifugation at 5000× g for 5 min and washing with H<sub>2</sub>O and absolute ethanol. SiO<sub>2</sub>-Pol(Lys) NPs were also synthesized via the same method except the incorporation of Ce.

COx@Ce@SiO<sub>2</sub> NGs were prepared by mixing Ce@SiO<sub>2</sub> NGs with several concentrations of COx (0.025, 0.05, 0.1, 0.2, and 0.4 mg/mL) for 30 min at RT. The samples were collected by centrifugation at 5000× g for 5 min, followed by washing with DI water to

obtain COx@Ce@SiO<sub>2</sub> NGs. The concentrations of COx before and after the immobilization remaining in the supernatant were measured using the bicinchoninic acid (BCA) assay to calculate the loading capacity.

#### 2.4. Evaluation of Peroxidase-like Activity of Ce@SiO<sub>2</sub> NGs

Peroxidase-like activity of Ce@SiO<sub>2</sub> NGs was assessed by monitoring the oxidation of TMB in the presence of H<sub>2</sub>O<sub>2</sub>. In this assay, Ce@SiO<sub>2</sub> NGs (0.1 mg/mL) were added into a reaction buffer (0.1 M sodium acetate (NaAc), pH 4.0) containing TMB (1 mM) and H<sub>2</sub>O<sub>2</sub> (10 mM) and incubated for 5 min at RT. Following the incubation, the catalytic materials were separated by centrifugation (13,000× *g*, 2 min). The absorbance of the supernatant was measured in a scanning mode from 550 to 750 nm or at 652 nm using a microplate reader (Synergy H1, BioTek, Winooski, VT, USA).

Stability of Ce@SiO<sub>2</sub> NGs was compared with that of HRP by evaluating their activity in NaAc buffer (0.1 M) across varying conditions of temperature (4 to 90 °C) and pH (3 to 9). After incubation for 2 h, the residual activities of Ce@SiO<sub>2</sub> NGs and HRP were measured using aforementioned colorimetric assays.

Steady-state kinetic studies were conducted to evaluate the kinetic parameters of Ce@SiO<sub>2</sub> NGs. The experiments were performed in NaAc buffer (0.1 M, pH 4.0) containing 0.1 mg/mL Ce@SiO<sub>2</sub> NGs. For TMB, the reaction buffer was supplemented with 10 mM H<sub>2</sub>O<sub>2</sub> at varying concentrations of TMB, while, for H<sub>2</sub>O<sub>2</sub>, 1 mM TMB was added in reaction buffer at various concentrations of H<sub>2</sub>O<sub>2</sub>. After addition of TMB or H<sub>2</sub>O<sub>2</sub>, absorbance was monitored by measuring the color changes of reaction solution using a kinetic mode at 652 nm. The kinetic parameters were calculated using the equation  $v = V_{max} \times [S] / (K_m + [S])$ , where *v* is the initial velocity, *V<sub>max</sub>* is maximal velocity, [S] is substrate concentration, and *K<sub>m</sub>* is Michaelis constant.

#### 2.5. Quantitative Determination of H<sub>2</sub>O<sub>2</sub> Using Ce@SiO<sub>2</sub> NGs

H<sub>2</sub>O<sub>2</sub> concentration was determined using TMB as a substrate in a transparent 96-well plate as follows. Various concentrations of H<sub>2</sub>O<sub>2</sub> were added in NaAc buffer (0.1 M, pH 4.0) containing Ce@SiO<sub>2</sub> NGs (0.1 mg/mL) and TMB (1 mM). After incubation for 5 min at RT, the Ce@SiO<sub>2</sub> NGs were separated and the absorbance of supernatant was measured at 652 nm using a microplate reader.

#### 2.6. Quantitative Determination of Choline Using COx@Ce@SiO<sub>2</sub> NGs

The quantification of choline level was conducted by incubating COx@Ce@SiO<sub>2</sub> NGs with varying concentrations of choline in HEPES buffer (0.05 M, pH 7.0) at RT for 15 min. Then, NaAc buffer (0.1 M, pH 4) containing 1 mM TMB was added and incubated for 5 min. Following the incubation, further procedures were the same as those described for H<sub>2</sub>O<sub>2</sub> detection.

#### 2.7. Detection of H<sub>2</sub>O<sub>2</sub> and Choline in Milk and Infant Formula Samples

Fresh milk and infant formula samples were purchased from local market and pre-treated with methanol to remove organic impurities before being diluted 100 times with HEPES buffer. The amounts of H<sub>2</sub>O<sub>2</sub> and choline in diluted samples were measured by HRP-TMB-based assay and choline assay kit (Abcam, Cambridge, UK), respectively. Then the prescribed amounts of H<sub>2</sub>O<sub>2</sub> (25, 50, and 100 μM) and choline (50, 100, and 200 μM) were added into diluted samples to create spiked samples. The levels of choline and H<sub>2</sub>O<sub>2</sub> in these spiked samples were subsequently analyzed using the same detection protocols as described earlier for individual H<sub>2</sub>O<sub>2</sub> and choline quantification. To evaluate the accuracy and reproducibility of the assay, recovery rate (%) and coefficient of variation (CV, %) were calculated based on three independent assay results for each spiked sample. Recovery rate (%) and CV (%) are defined by these equations: [recovery (%) = measured value/actual value × 100] and [CV (%) = SD/average × 100].

### 3. Results and Discussion

#### 3.1. Synthesis and Characterization of Ce@SiO<sub>2</sub> NGs

Peroxidase-like Ce@SiO<sub>2</sub> NGs, synthesized via a biocatalytic ATRP reaction, were used to construct cascade nanozyme COx@Ce@SiO<sub>2</sub> NGs by entrapping COx for the convenient colorimetric detection of choline (Figure 1). The morphological characteristics of the Ce@SiO<sub>2</sub> NGs were analyzed using SEM, which revealed a notable change in the dispersion of the SiO<sub>2</sub> NPs after the polymer brush incorporation (Figure 2a,b). The bare SiO<sub>2</sub> NPs were highly dispersed, while the Ce@SiO<sub>2</sub> NGs displayed marginal aggregation, suggesting successful coating with the polymer brushes. The TEM images also showed a uniform spherical morphology with a diameter of approximately 160 nm of the bare SiO<sub>2</sub> NPs (Figure 2c). After the surface modification, the Ce@SiO<sub>2</sub> NGs exhibited an enlarged particle size due to the formation of outer polymeric brushes, with ~25 nm thickness, on the SiO<sub>2</sub> core (Figure 2d). The EDS analysis validated the presence of C, O, N, Si, and Ce elements within the Ce@SiO<sub>2</sub> NGs (Figure 2e), confirming the successful incorporation of the Ce ions in the nanogel matrix. The FT-IR spectroscopy further confirmed the successful synthesis of the Ce@SiO<sub>2</sub> NGs (Figure 2f). The presence of Si-O-Si linkages was evident from the strong absorption peaks observed between 800 and 1100 cm<sup>-1</sup>, one of the characteristics of silica networks. Additional peaks at 1521 cm<sup>-1</sup>, 1635 cm<sup>-1</sup>, 3143 cm<sup>-1</sup>, and 3354 cm<sup>-1</sup> were attributed to the stretching vibrations of C=O, C-H, N-H, and O-H, respectively, indicating the presence of the functional groups associated with the polymeric network and Ce coordination [26–28]. In addition, the XPS full spectra for the Ce@SiO<sub>2</sub> NGs revealed the presence of C, O, N, Si, and Ce elements, which is consistent with the EDS analysis (Figure S1). The high-resolution XPS spectra presented special peaks of Si 2p, N 1s (N-H, C-N), and Ce 3d, which were observed at 103.1, 399.2, and 401.2, respectively [33,34]. The Ce@SiO<sub>2</sub> NGs showed an extremely hydrophilic property, demonstrated by the contact angle of ~16°, which was 3-fold smaller than that of the SiO<sub>2</sub> NPs (Figure S2). The enhanced hydrophilicity of the Ce@SiO<sub>2</sub> NGs is presumed by the carboxyl and hydroxyl groups on their surface, which was confirmed by the FT-IR analysis. These spectral features collectively confirm the successful formation of Ce-coordinated nanogels with the intended structural and functional characteristics.

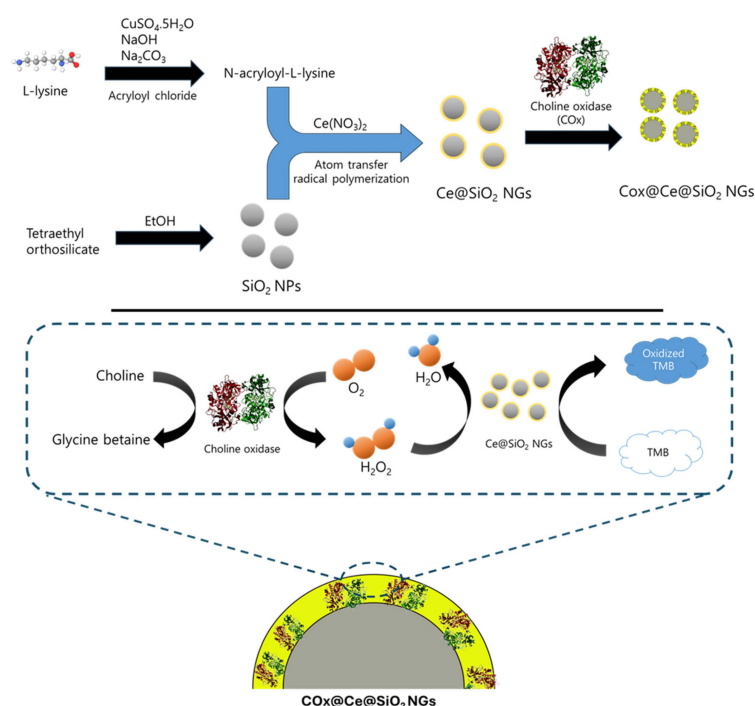


**Figure 1.** Schematic illustration for the synthesis of Ce@SiO<sub>2</sub> NGs and COx@Ce@SiO<sub>2</sub> NGs, with their applications to colorimetrically detect H<sub>2</sub>O<sub>2</sub> and choline.

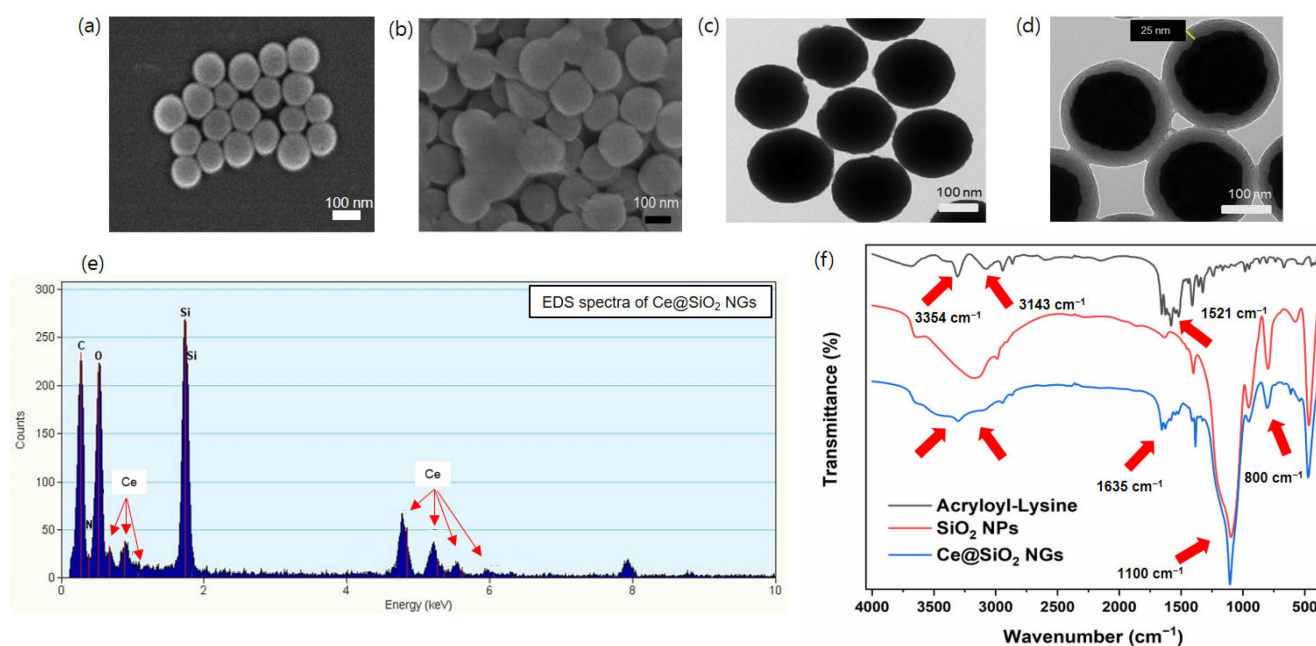


**Figure 2.** SEM images of (a) SiO<sub>2</sub> NPs and (b) Ce@SiO<sub>2</sub> NGs. TEM images of (c) SiO<sub>2</sub> NPs and (d) Ce@SiO<sub>2</sub> NGs. (e) EDS and (f) FT-IR spectra of Ce@SiO<sub>2</sub> NGs.

### 3.2. Investigation of Peroxidase-like Activity of Ce@SiO<sub>2</sub> NGs

The peroxidase-like activity of the Ce@SiO<sub>2</sub> NGs was evaluated by performing the peroxidase-mediated oxidation of TMB in the presence of H<sub>2</sub>O<sub>2</sub>. First, the influences of pH and temperature on the catalytic activity were explored. The results showed that the Ce@SiO<sub>2</sub> NGs exhibited their maximal activity at pH 4.0 and 37 °C (Figure S3a,b); however, to facilitate practical utilizations, RT was used in further assays where the activity was more than 80% of that observed at 37 °C. During only a 5 min reaction, the Ce@SiO<sub>2</sub> NGs successfully catalyzed the oxidation of TMB, producing a strong blue color signal in the presence of H<sub>2</sub>O<sub>2</sub>, but showed no activity without H<sub>2</sub>O<sub>2</sub> (Figure 3). In addition, the incorporation of Ce ions within the SiO<sub>2</sub> NPs played a key role in mimicking the peroxidase activity when SiO<sub>2</sub>-Pol(Lys) NPs, as a control, did not oxidize TMB in the presence of H<sub>2</sub>O<sub>2</sub> (Figure S4). Moreover, the Ce@SiO<sub>2</sub> NGs exhibited remarkable stability across broad pH and temperature ranges, contrasting with HRP, which rapidly lost activity under acidic conditions and elevated temperatures (Figure S3c,d). During the catalytic action of the Ce@SiO<sub>2</sub> NGs in the presence of H<sub>2</sub>O<sub>2</sub>, the production of hydroxyl radicals was confirmed by employing a terephthalic acid (TA) probe, indicating that TMB can be oxidized with the hydroxyl radicals, similar to HRP-mediated catalysis (Figure S5). These results proved that trapped Ce ions within SiO<sub>2</sub> NPs using a biocatalytic ATRP reaction notably enhanced the peroxidase-like activity and stability, which may serve as a feasible alternative to HRP in versatile applications.

To fully elucidate the peroxidase activity of the Ce@SiO<sub>2</sub> NGs, their steady-state kinetic parameters were determined. The results showed that the Ce@SiO<sub>2</sub> NGs followed Michaelis–Menten kinetics for both TMB and H<sub>2</sub>O<sub>2</sub> (Figure S6a,b), and the kinetic parameters,  $K_m$  and  $V_{max}$ , were determined via Lineweaver–Burk plots (Figure S6c,d). Importantly, the  $K_m$  values of the Ce@SiO<sub>2</sub> NGs for TMB and H<sub>2</sub>O<sub>2</sub> were found to be 0.57 and 1.79 mM, respectively, demonstrating a strong affinity when compared with other conventional nanozymes and HRP (Table S1). The enhanced affinity may be due to the polymeric brushes located outside the nanogels, which provide dynamic microenvironments around coordinated Ce ions, providing improved hydrophilicity and facilitating substrate transfer to the active site of the Ce@SiO<sub>2</sub> NGs. These kinetic parameters demonstrate the high catalytic efficiency of Ce@SiO<sub>2</sub> NGs, highlighting their potential as a robust alternative to

natural HRP for the colorimetric detection of  $H_2O_2$  and biomarkers in various analytical applications.

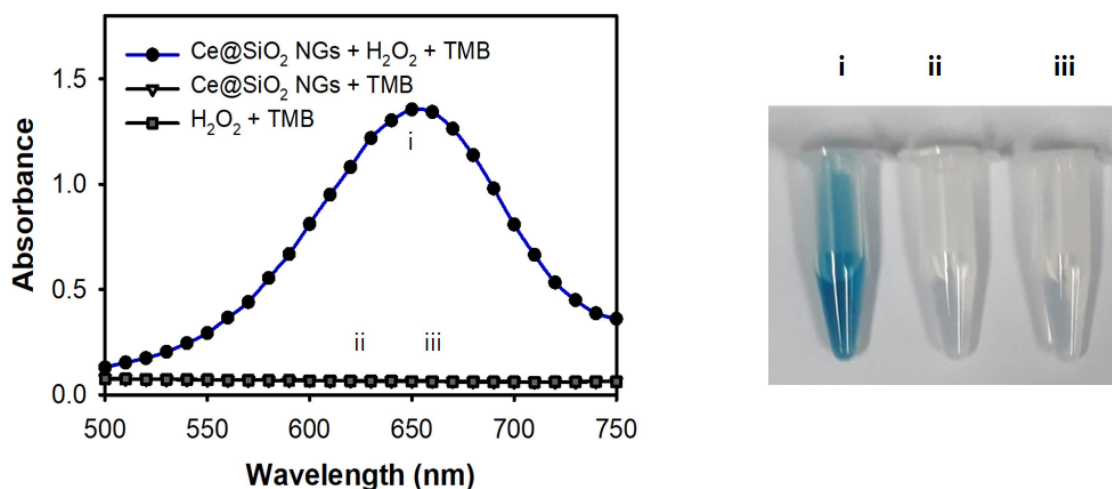


**Figure 3.** Peroxidase-like activity of  $Ce@SiO_2$  NGs through the oxidation of TMB in the presence of  $H_2O_2$ . The assay was performed in NaAc buffer (0.1 M, pH 4) containing  $Ce@SiO_2$  NGs (0.1 mg/mL) and TMB (1 mM) for 5 min incubation at RT. Sample specifications: i:  $Ce@SiO_2$  NGs +  $H_2O_2$  + TMB, ii:  $Ce@SiO_2$  NGs + TMB, and iii:  $H_2O_2$  + TMB.

### 3.3. Quantitative Detection of $H_2O_2$ Using $Ce@SiO_2$ NGs

The oxidation of TMB via  $H_2O_2$  catalyzed by  $Ce@SiO_2$  NGs produces a vivid blue color signal, directly proportional to the concentration of  $H_2O_2$ . Leveraging this reaction, a colorimetric strategy for  $H_2O_2$  detection using  $Ce@SiO_2$  NGs was developed. As a result,  $H_2O_2$  was specifically detected during a 5 min reaction, whereas no significant color change was observed for the negative control samples, such as glucose, cholesterol, glutathione (GSH), histidine, bovine serum albumin (BSA),  $Fe^{2+}$ , and NaCl, at the same concentration with  $H_2O_2$  (5 mM), confirming the excellent specificity of the assay system towards the target  $H_2O_2$  (Figure 4a). The limit of detection (LOD) value was calculated using the formula  $LOD = 3 \times \delta / \text{slope}$ , where  $\delta$  is the standard deviation of the blank and slope is the slope of the calibration curve. Through the analysis of the dose–response curve, the LOD for  $H_2O_2$  was determined to be as low as 1.3  $\mu M$ , with a linear range from 5 to 1000  $\mu M$  (Figure 4b). The LOD and linear range values are among the most sensitive reported for colorimetric  $H_2O_2$  detection, making this system highly advantageous for quantifying  $H_2O_2$  and other biomarkers when combined with their respective oxidase enzymes (Table 1).

**Table 1.** Comparison of analytical performances of various nanozymes for  $H_2O_2$  detection.

| Sample                         | Linear Range ( $\mu M$ ) | LOD ( $\mu M$ ) | References |
|--------------------------------|--------------------------|-----------------|------------|
| Poly(ANI-co-AA) composite film | 25–200                   | 35.6            | [35]       |
| $Fe_3O_4$ QDs                  | 10–400                   | 4.5             | [36]       |
| CS@GSH-CuNCs                   | 20–200                   | 6.7             | [37]       |
| Au/ $Co_3O_4$ -CeOx NCs        | 10–100                   | 5.29            | [38]       |
| Fe-Ag <sub>2</sub> S           | 10–150                   | 7.82            | [39]       |
| Ag@TPE-SiO <sub>2</sub> NPs    | 5–160                    | 2.1             | [40]       |
| Co/CeO <sub>2</sub>            | 3.33–100                 | 3.33            | [41]       |
| $Ce@SiO_2$ NGs                 | 5–1000                   | 1.3             | This work  |

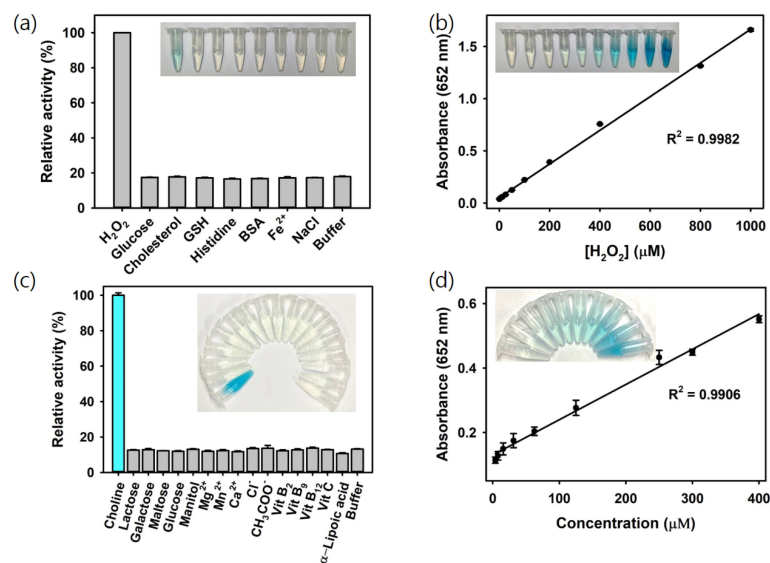


**Figure 4.** (a) Selectivity and (b) linear calibration plots to show sensitivity for the colorimetric detection of  $\text{H}_2\text{O}_2$  using  $\text{Ce@SiO}_2$  NGs. (c) Selectivity and (d) linear calibration plots to show sensitivity for the colorimetric detection of choline using  $\text{COx@SiO}_2$  NGs.

### 3.4. Quantitative Detection of Choline Using $\text{COx@Ce@SiO}_2$ NGs

$\text{H}_2\text{O}_2$  is a byproduct of the natural oxidase-mediated catalysis of biomarkers, and the  $\text{COx@SiO}_2$  NG-based system exhibited high selectivity and sensitivity in detecting  $\text{H}_2\text{O}_2$ . Based on these observations, we developed a detection system for choline, an important neurotransmitter and biomarker for monitoring various diseases and nutritional status, by incorporating COx into  $\text{Ce@SiO}_2$  NGs to construct  $\text{COx@Ce@SiO}_2$ . In the presence of choline, the entrapped COx catalyzes the oxidation of choline to produce  $\text{H}_2\text{O}_2$ , which subsequently activates the peroxidase-mimicking  $\text{Ce@SiO}_2$  to produce a visible blue color signal from the oxidation of TMB. To optimize the preparation conditions of  $\text{COx@Ce@SiO}_2$ , we investigated the effects of the COx concentration on its loading and choline detecting activity (Figure S7). The porous nature of the  $\text{Ce@SiO}_2$  NGs is expected to be advantageous to entrap COx, and, at 0.1 mg/mL COx, the maximum loading (~28 wt%) and activity were achieved, indicating that this concentration is optimal for the formation of  $\text{COx@Ce@SiO}_2$  NGs.

Using the optimized conditions with the  $\text{COx@Ce@SiO}_2$  NGs, choline was specifically detected by the intense blue color produced, while no noticeable color change occurred in the negative controls, including common interferes in milk such as lactose, galactose, maltose, glucose, manitol,  $\text{Mg}^{2+}$ ,  $\text{Mn}^{2+}$ ,  $\text{Ca}^{2+}$ ,  $\text{Cl}^-$ ,  $\text{CH}_3\text{COO}^-$ , vitamin B<sub>2</sub>, B<sub>9</sub>, B<sub>12</sub>, C, and  $\alpha$ -lipoic acid, demonstrating the high specificity of the  $\text{COx@Ce@SiO}_2$  NG-based system towards choline (Figure 4c). The linear calibration plots showed the LOD as low as 2  $\mu\text{M}$ , with a linear range from 4 to 400  $\mu\text{M}$  (Figure 4d). These LOD and linear range values rank among the most sensitive reported for colorimetric choline detection (Table 2). These results proved that the developed biosensor could serve as a simple and highly sensitive approach for  $\text{H}_2\text{O}_2$  and choline analysis without using expensive and specialized instruments or complex labeling procedures, making it a valuable tool for choline and food safety analysis in dairy products and infant nutrition.

**Table 2.** Comparison of analytical performances of various nanozymes for choline detection.

| Sample                | Linear Range ( $\mu\text{M}$ ) | LOD ( $\mu\text{M}$ ) | References |
|-----------------------|--------------------------------|-----------------------|------------|
| Au/HZIF-8@TCPP(Fe)    | 50–2000                        | 50                    | [42]       |
| $\text{ChO}_x$ @MOF   | 6–300                          | 2                     | [43]       |
| Mn/ZIF-90             | 5–50 and 50–1000               | 5.6                   | [44]       |
| CS@GSH-CuNCs          | 20–150                         | 6.5                   | [37]       |
| $\text{Ce@SiO}_2$ NGs | 4–400                          | 2                     | This work  |



The storage stabilities of the COx@Ce@SiO<sub>2</sub> NGs and a free enzyme system comprising free HRP and free COx were evaluated under different temperature conditions (4 °C, RT, and 37 °C). The results showed the improved stability of the COx@Ce@SiO<sub>2</sub> NGs under different temperature conditions (Figure S8), which may be attributed to the protective polymeric brushes of the nanogel. When nanogels were employed, the choline detecting activity was maintained over 80% during 6 days at RT, whereas the free system lost over 40% of its initial activity. When stored at 37 °C, there was a marginal decrease in the COx@Ce@SiO<sub>2</sub> NGs, probably due to the temperature-dependent denaturation and release of the immobilized COx.

### 3.5. Choline and H<sub>2</sub>O<sub>2</sub> Detection in Milk and Infant Formula Samples

Choline is predominantly found in infant formula and fresh milk, making its accurate detection crucial for ensuring nutritional quality. To assess the practical applicability of the COx@Ce@SiO<sub>2</sub> NG-based assay, commercially available milk and infant formula were used to prepare the spiked sample for analysis. Initially, the original concentrations of choline in the fresh samples were determined using commercial assay kits, followed by the addition of specific amounts of choline to prepare the spiked samples. As a result, the choline levels in the spiked samples were measured with high precision and accuracy, with CVs in the range of 0.3 to 4.1% and recoveries of 97.5 to 105.3%. Additionally, the NGs designed for H<sub>2</sub>O<sub>2</sub> detection demonstrated great analytical performance, with recoveries for the spiked H<sub>2</sub>O<sub>2</sub> in the milk and infant formula samples ranging from 97.5 to 103.7% and CVs between 1.2 and 4.0%, underscoring the method's reliability and reproducibility (Table 3). These results highlight the capability of using the COx@Ce@SiO<sub>2</sub> NG-based assay to effectively analyze real food matrices, such as dairy products, ensuring the safety and nutritional adequacy of infant food sources.

**Table 3.** Detection precision of COx@Ce@SiO<sub>2</sub> NGs and Ce@SiO<sub>2</sub> NGs for choline and H<sub>2</sub>O<sub>2</sub> quantification, respectively, in spiked milk and infant formula samples.

|                               |                   | Original Amount (μM) | Spiked Level (μM) | Measured (μM) | Recovery (%) (n = 3) | CV (%) |
|-------------------------------|-------------------|----------------------|-------------------|---------------|----------------------|--------|
| Choline                       | Milk #1           | 7.9                  | 50                | 57.0          | 98.4                 | 3.2    |
|                               |                   |                      | 100               | 111.0         | 102.8                | 3.6    |
|                               |                   |                      | 200               | 209.8         | 100.9                | 0.3    |
|                               | Milk #2           | 6.6                  | 50                | 57.2          | 101.1                | 2.3    |
|                               |                   |                      | 100               | 103.9         | 97.5                 | 1.3    |
|                               |                   |                      | 200               | 204.7         | 99.1                 | 1.0    |
|                               | Infant formula #1 | 8.2                  | 50                | 59.2          | 101.8                | 3.8    |
|                               |                   |                      | 100               | 111.4         | 103.0                | 1.1    |
|                               |                   |                      | 200               | 214.0         | 102.8                | 2.1    |
|                               | Infant formula #2 | 8.1                  | 50                | 57.6          | 99.2                 | 3.6    |
|                               |                   |                      | 100               | 109.3         | 101.1                | 4.1    |
|                               |                   |                      | 200               | 219.0         | 105.3                | 2.4    |
| H <sub>2</sub> O <sub>2</sub> | Milk #1           | 0                    | 25                | 25.9          | 103.7                | 1.8    |
|                               |                   |                      | 50                | 50.8          | 101.5                | 1.2    |
|                               |                   |                      | 100               | 99.5          | 99.5                 | 2.7    |
|                               | Milk #2           | 0                    | 25                | 25.24         | 101.0                | 2.5    |
|                               |                   |                      | 50                | 49.4          | 98.8                 | 3.6    |
|                               |                   |                      | 100               | 101.8         | 101.8                | 2.7    |
|                               | Infant formula #1 | 0                    | 25                | 25.7          | 103.0                | 2.4    |
|                               |                   |                      | 50                | 50.4          | 100.8                | 4.0    |
|                               |                   |                      | 100               | 97.5          | 97.5                 | 2.7    |
|                               | Infant formula #2 | 0                    | 25                | 25.1          | 100.3                | 2.5    |
|                               |                   |                      | 50                | 51.3          | 102.6                | 3.1    |
|                               |                   |                      | 100               | 100.6         | 100.6                | 2.6    |

#### 4. Conclusions

We demonstrated that Ce@SiO<sub>2</sub> NGs and COx@Ce@SiO<sub>2</sub> NGs present a significant advancement in the colorimetric detection of H<sub>2</sub>O<sub>2</sub> and choline, respectively. The ATRP-based synthesis of Ce@SiO<sub>2</sub> NGs resulted in well-defined polymer-coated nanoparticles with excellent peroxidase-like activity. High selectivity and sensitivity towards target H<sub>2</sub>O<sub>2</sub> and choline were achieved, underscoring their applicability in real-world scenarios. Validation through assays using commercial milk and infant formula confirmed the reliability and accuracy in practical applications. This research highlights the potential of ATRP-based nanozymes not only for enhancing food safety analysis in dairy products but also for broader biosensing applications, paving the way for future nanozymatic innovations in this field.

**Supplementary Materials:** The following supporting information can be downloaded at <https://www.mdpi.com/article/10.3390/bios14120563/s1>, Figure S1: XPS spectra of (a) Ce@SiO<sub>2</sub> NGs and their high-resolution XPS spectra of (b) Si 2p, (c) N 1s, and (d) Ce 3d; Figure S2: Contact angle of (a) SiO<sub>2</sub> NPs and (b) Ce@SiO<sub>2</sub> NGs; Figure S3: Effects of (a) pH and (b) temperature on the peroxidase-like activity of Ce@SiO<sub>2</sub> NGs. Catalytic stabilities of Ce@SiO<sub>2</sub> NGs and HRP in ranges of (c) pH and (d) temperature; Figure S4: Peroxidase-like activity of (i) Ce@SiO<sub>2</sub> NGs, (ii) SiO<sub>2</sub>-Pol(Lys) NPs, and (iii) 10 mM H<sub>2</sub>O<sub>2</sub>; Figure S5: Demonstration of hydroxyl radicals produced during the catalytic action of Ce@SiO<sub>2</sub> NGs and HRP in the presence of H<sub>2</sub>O<sub>2</sub>. In the assays, 10 mM H<sub>2</sub>O<sub>2</sub> and 0.625 mM TA were employed; Figure S6: Steady-state kinetic assays of Ce@SiO<sub>2</sub> NGs for (a) TMB and (b) H<sub>2</sub>O<sub>2</sub> and their corresponding double reciprocal (Lineweaver–Burk) plots of activity; Figure S7: (a) COx loading percentage within Ce@SiO<sub>2</sub> NGs (1mg/mL) and (b) relative activity to detect choline prepared at various initial COx concentrations; Figure S8: Storage stability of (a) free enzyme system comprising free HRP and free COx and (b) COx@Ce@SiO<sub>2</sub> NGs under different temperature conditions; Table S1: Comparison of peroxidase-like kinetic parameters of Ce@SiO<sub>2</sub> NGs and other catalysts. References [45,46] are cited in the Supplementary Materials.

**Author Contributions:** Conceptualization, investigation, writing—original draft preparation, T.H.V.; investigation, validation, writing—review and editing, B.J.Y.; and conceptualization, supervision, writing—review and editing, M.I.K. All authors have read and agreed to the published version of the manuscript.

**Funding:** This work was supported by a National Research Foundation of Korea (NRF) grant funded by the Korean government (Ministry of Science and ICT [NRF-2023R1A2C2007833]) and the Basic Science Research Program through the NRF funded by the Ministry of Education (Grant No. 2021R1A6A1A03038996). This study has also been conducted with the support of the Korea Institute of Industrial Technology as “Development of nano material and process for smart living sensor (KITECH EO-24-0003)”.

**Informed Consent Statement:** Not applicable.

**Data Availability Statement:** Data are contained within the article and Supplementary Materials.

**Conflicts of Interest:** The authors declare no conflicts of interest.

#### References

1. Zeisel, S.H. Nutritional importance of choline for brain development. *J. Am. Coll. Nutr.* **2004**, *23* (Suppl. S6), 621S–626S. [CrossRef]
2. Moretti, A.; Paoletta, M.; Liguori, S.; Bertone, M.; Toro, G.; Iolascon, G. Choline: An essential nutrient for skeletal muscle. *Nutrients* **2020**, *12*, 2144. [CrossRef]
3. Cater, R.J.; Mukherjee, D.; Gil-Iturbe, E.; Erramilli, S.K.; Chen, T.; Koo, K.; Santander, N.; Reckers, A.; Kloss, B.; Gawda, T.; et al. Structural and molecular basis of choline uptake into the brain by FLVCR2. *Nature* **2024**, *629*, 704–709. [CrossRef]
4. Arai, T.; Tanaka, M.; Goda, N. HIF-1-dependent lipin1 induction prevents excessive lipid accumulation in choline-deficient diet-induced fatty liver. *Sci. Rep.* **2018**, *8*, 14230. [CrossRef]
5. Velazquez, R.; Ferreira, E.; Winslow, W.; Dave, N.; Piras, I.S.; Naymik, M.; Huentelman, M.J.; Tran, A.; Caccamo, A.; Oddo, S. Maternal choline supplementation ameliorates Alzheimer’s disease pathology by reducing brain homocysteine levels across multiple generations. *Mol. Psychiatry* **2020**, *25*, 2620–2629. [CrossRef]
6. Abd El-Rahman, M.K.; Mazzone, G.; Mahmoud, A.M.; Sicilia, E.; Shoeib, T. Novel choline selective electrochemical membrane sensor with application in milk powders and infant formulas. *Talanta* **2021**, *221*, 121409. [CrossRef]

7. Mathivanan, D.; Devi, K.S.; Sathiyar, G.; Tyagi, A.; da Silva, V.; Janegitz, B.; Prakash, J.; Gupta, R.K. Novel polypyrrole-graphene oxide-gold nanocomposite for high performance hydrogen peroxide sensing application. *Sens. Actuator A-Phys.* **2021**, *328*, 112769. [[CrossRef](#)]
8. Giaretta, J.E.; Duan, H.; Farajikhah, S.; Oveissi, F.; Dehghani, F.; Naficy, S. A highly flexible, physically stable, and selective hydrogel-based hydrogen peroxide sensor. *Sens. Actuator B-Chem.* **2022**, *371*, 132483. [[CrossRef](#)]
9. Tian, X.; Qin, Y.; Jiang, Y.; Guo, X.; Wen, Y.; Yang, H. Chemically renewable SERS sensor for the inspection of H<sub>2</sub>O<sub>2</sub> residue in food stuff. *Food Chem.* **2024**, *438*, 137777. [[CrossRef](#)]
10. Nguyen, T.D.; Nguyen, M.H.; Vu, M.T.; Duong, H.A.; Pham, H.V.; Mai, T.D. Dual-channeled capillary electrophoresis coupled with contactless conductivity detection for rapid determination of choline and taurine in energy drinks and dietary supplements. *Talanta* **2019**, *193*, 168–175. [[CrossRef](#)]
11. Giaretta, J.E.; Oveissi, F.; Dehghani, F.; Naficy, S. Paper-Based, Chemiresistive Sensor for Hydrogen Peroxide Detection. *Adv. Mater. Technol.* **2021**, *6*, 2001148. [[CrossRef](#)]
12. Wu, W.; Huang, L.; Wang, E.; Dong, S. Atomic engineering of single-atom nanozymes for enzyme-like catalysis. *Chem. Sci.* **2020**, *11*, 9741–9756. [[CrossRef](#)]
13. Shamsabadi, A.; Haghighi, T.; Carvalho, S.; Frenette, L.C.; Stevens, M.M. The nanozyme revolution: Enhancing the performance of medical biosensing platforms. *Adv. Mater.* **2024**, *36*, 2300184. [[CrossRef](#)]
14. Nguyen, P.T.; Lee, J.; Cho, A.; Kim, M.S.; Choi, D.; Han, J.W.; Kim, M.I.; Lee, J. Rational development of co-doped mesoporous ceria with high peroxidase-mimicking activity at neutral pH for paper-based colorimetric detection of multiple biomarkers. *Adv. Funct. Mater.* **2022**, *32*, 2112428. [[CrossRef](#)]
15. Vu, T.H.; Nguyen, P.T.; Kim, M.I. Polydopamine-coated Co<sub>3</sub>O<sub>4</sub> nanoparticles as an efficient catalase mimic for fluorescent detection of sulfide ion. *Biosensors* **2022**, *12*, 1047. [[CrossRef](#)]
16. Lee, J.; Le, X.A.; Chun, H.; Vu, T.H.; Choi, D.; Han, B.; Kim, M.I.; Lee, J. Active site engineering of Zn-doped mesoporous ceria toward highly efficient organophosphorus hydrolase-mimicking nanozyme. *Biosens. Bioelectron.* **2024**, *246*, 115882. [[CrossRef](#)]
17. Nguyen, P.T.; Vu, T.H.; Kim, M.I. Histidine–cysteine–copper hybrid nanoflowers as active site-inspired laccase mimics for the colorimetric detection of phenolic compounds in PDMS microfluidic devices. *Sens. Actuator B-Chem.* **2024**, *413*, 135845. [[CrossRef](#)]
18. Tian, Q.; Li, S.; Tang, Z.; Zhang, Z.; Du, D.; Zhang, X.; Niu, X.; Lin, Y. Nanozyme-enabled biomedical diagnosis: Advances, trends, and challenges. *Adv. Healthc. Mater.* **2024**, 2401630. [[CrossRef](#)]
19. Zhang, S.; Wei, Q.; Shang, Y.; Zhang, Q.; Wang, Q. D-Serine enzymatic metabolism induced formation of a powder-remoldable PAAM–CS hydrogel. *Chem. Commun.* **2017**, *53*, 12270–12273. [[CrossRef](#)]
20. Cui, Z.-K.; Kim, S.; Baljon, J.J.; Wu, B.M.; Aghaloo, T.; Lee, M. Microporous methacrylated glycol chitosan-montmorillonite nanocomposite hydrogel for bone tissue engineering. *Nat. Commun.* **2019**, *10*, 3523. [[CrossRef](#)]
21. Nguyen, P.T.; Ahn, H.T.; Kim, M.I. Reagent-free colorimetric assay for galactose using agarose gel entrapping nanoceria and galactose oxidase. *Nanomaterials* **2020**, *10*, 895. [[CrossRef](#)]
22. Kim, M.I.; Park, C.Y.; Seo, J.M.; Kang, K.S.; Park, K.S.; Kang, J.; Hong, K.S.; Choi, Y.; Lee, S.Y.; Park, J.P.; et al. In situ biosynthesis of a metal nanoparticle encapsulated in alginate gel for imageable drug-delivery system. *ACS Appl. Mater. Interfaces* **2021**, *13*, 36697–36708. [[CrossRef](#)]
23. Nguyen, Q.H.; Lee, D.H.; Nguyen, P.T.; Le, P.G.; Kim, M.I. Foldable paper microfluidic device based on single iron site-containing hydrogel nanozyme for efficient glucose biosensing. *Chem. Eng. J.* **2023**, *454*, 140541. [[CrossRef](#)]
24. Qi, M.; Pan, H.; Shen, H.; Xia, X.; Wu, C.; Han, X.; He, X.; Tong, W.; Wang, X.; Wang, Q. Nanogel multienzyme mimics synthesized by biocatalytic ATRP and metal coordination for bioresponsive fluorescence imaging. *Angew. Chem.-Int. Ed.* **2020**, *132*, 11846–11851. [[CrossRef](#)]
25. Wang, H.; Liu, X.; Yan, X.; Du, Y.; Pu, F.; Ren, J.; Qu, X. An ATPase-Mimicking MXene nanozyme pharmacologically breaks the iron-clad defense system for ferroptosis cancer therapy. *Biomaterials* **2024**, *307*, 122523. [[CrossRef](#)] [[PubMed](#)]
26. Kaygusuz, H.; Torlak, E.; Akın-Evingür, G.; Özen, İ.; Von Klitzing, R.; Erim, F.B. Antimicrobial cerium ion-chitosan crosslinked alginate biopolymer films: A novel and potential wound dressing. *Int. J. Biol. Macromol.* **2017**, *105*, 1161–1165. [[CrossRef](#)]
27. Ma, T.; Zhai, X.; Huang, Y.; Zhang, M.; Li, P.; Du, Y.J. Cerium ions crosslinked sodium alginate-carboxymethyl chitosan spheres with antibacterial activity for wound healing. *J. Rare Earths* **2022**, *40*, 1407–1416. [[CrossRef](#)]
28. Wei, Y.; Wang, L.; Wang, J. Cerium alginate cross-linking with biochar beads for fast fluoride removal over a wide pH range. *Colloid Surf. A-Physicochem. Eng. Asp.* **2022**, *636*, 128161. [[CrossRef](#)]
29. Li, X.-J.; Yan, C.-J.; Luo, W.-J.; Gao, Q.; Zhou, Q.; Liu, C.; Zhou, S. Exceptional cerium (III) adsorption performance of poly (acrylic acid) brushes-decorated attapulgite with abundant and highly accessible binding sites. *Chem. Eng. J.* **2016**, *284*, 333–342. [[CrossRef](#)]
30. Chen, Z.; Song, S.; Zeng, H.; Ge, Z.; Liu, B.; Fan, Z. 3D printing MOF nanozyme hydrogel with dual enzymatic activities and visualized glucose monitoring for diabetic wound healing. *Chem. Eng. J.* **2023**, *471*, 144649. [[CrossRef](#)]
31. Nosrati, H.; Heydari, M.; Khodaei, M. Cerium oxide nanoparticles: Synthesis methods and applications in wound healing. *Mater. Today Bio* **2023**, *23*, 100823. [[CrossRef](#)]
32. Othman, A.; Gowda, A.; Andreescu, D.; Hassan, M.H.; Babu, S.; Seo, J.; Andreescu, S. Two decades of ceria nanoparticles research: Structure, properties and emerging applications. *Mater. Horiz.* **2024**, *11*, 3213–3266. [[CrossRef](#)]

33. Ganganboina, A.B.; Doong, R.A. Nitrogen doped graphene quantum dot-decorated earth-abundant nanotubes for enhanced capacitive deionization. *Environ. Sci.-Nano* **2020**, *7*, 228–237. [[CrossRef](#)]
34. Anandan, C.; Bera, P. XPS studies on the interaction of CeO<sub>2</sub> with silicon in magnetron sputtered CeO<sub>2</sub> thin films on Si and Si<sub>3</sub>N<sub>4</sub> substrates. *Appl. Surf. Sci.* **2013**, *283*, 297–303. [[CrossRef](#)]
35. Hosu, O.; Lettieri, M.; Papara, N.; Ravalli, A.; Sandulescu, R.; Cristea, C.; Marrazza, G. Colorimetric multienzymatic smart sensors for hydrogen peroxide, glucose and catechol screening analysis. *Talanta* **2019**, *204*, 525–532. [[CrossRef](#)]
36. Li, P.; Zhang, S.; Xu, C.; Zhang, L.; Liu, Q.; Chu, S.; Li, S.; Mao, G.; Wang, H. Coating Fe<sub>3</sub>O<sub>4</sub> quantum dots with sodium alginate showing enhanced catalysis for capillary array-based rapid analysis of H<sub>2</sub>O<sub>2</sub> in milk. *Food Chem.* **2022**, *380*, 132188. [[CrossRef](#)]
37. Chen, S.; Li, Z.; Huang, Z.; Jia, Q. Investigation of efficient synergistic and protective effects of chitosan on copper nanoclusters: Construction of highly active and stable nanozyme for colorimetric and fluorometric dual-signal biosensing. *Sens. Actuator B-Chem.* **2021**, *332*, 129522. [[CrossRef](#)]
38. Liu, H.; Ding, Y.; Yang, B.; Liu, Z.; Liu, Q.; Zhang, X. Colorimetric and ultrasensitive detection of H<sub>2</sub>O<sub>2</sub> based on Au/Co<sub>3</sub>O<sub>4</sub>-CeO<sub>x</sub> nanocomposites with enhanced peroxidase-like performance. *Sens. Actuator B-Chem.* **2018**, *271*, 336–345. [[CrossRef](#)]
39. Ding, Y.; Liu, H.; Gao, L.-N.; Fu, M.; Luo, X.; Zhang, X.; Liu, Q.; Zeng, R.-C. Compounds. Fe-doped Ag<sub>2</sub>S with excellent peroxidase-like activity for colorimetric determination of H<sub>2</sub>O<sub>2</sub>. *J. Alloys Compd.* **2019**, *785*, 1189–1197. [[CrossRef](#)]
40. Huang, X.; Zhou, H.; Huang, Y.; Jiang, H.; Yang, N.; Shahzad, S.A.; Meng, L.; Yu, C. Silver nanoparticles decorated and tetraphenylethene probe doped silica nanoparticles: A colorimetric and fluorometric sensor for sensitive and selective detection and intracellular imaging of hydrogen peroxide. *Biosens. Bioelectron.* **2018**, *121*, 236–242. [[CrossRef](#)]
41. Remani, K.; Binitha, N.N. Cobalt doped ceria catalysts for the oxidative abatement of gaseous pollutants and colorimetric detection of H<sub>2</sub>O<sub>2</sub>. *Mater. Res. Bull.* **2021**, *139*, 111253. [[CrossRef](#)]
42. Zhang, H.; Wu, H.; Qin, X.; Shen, Y.; Wei, X.; Liu, G. Metalloporphyrin and gold nanoparticles modified hollow zeolite imidazole Framework-8 with excellent peroxidase like activity for quick colorimetric determination of choline in infant formula milk powder. *Food Chem.* **2022**, *384*, 132552. [[CrossRef](#)] [[PubMed](#)]
43. Huang, H.; Song, D.; Zhang, W.; Fang, S.; Zhou, Q.; Zhang, H.; Liang, Z.; Li, Y.J. Choline oxidase-integrated copper metal-organic frameworks as cascade nanozymes for one-step colorimetric choline detection. *J. Agric. Food Chem.* **2022**, *70*, 5228–5236. [[CrossRef](#)] [[PubMed](#)]
44. Wang, J.-L.; Chen, G.-Y.; Chai, T.-Q.; Chen, L.-X.; Chen, H.; Yang, F.-Q. Construction of Mn-decorated zeolitic imidazolate framework-90 nanostructure as superior oxidase-like mimic for colorimetric detection of glucose and choline. *Talanta* **2024**, *271*, 125708. [[CrossRef](#)]
45. Alizadeh, N.; Salimi, A.; Hallaj, R. Mimicking peroxidase-like activity of Co<sub>3</sub>O<sub>4</sub>-CeO<sub>2</sub> nanosheets integrated paper-based analytical devices for detection of glucose with smartphone. *Sens. Actuator B-Chem.* **2019**, *288*, 44–52. [[CrossRef](#)]
46. Gao, L.; Zhuang, J.; Nie, L.; Zhang, J.; Zhang, Y.; Gu, N.; Wang, T.; Feng, J.; Yang, D.; Perrett, S. Intrinsic peroxidase-like activity of ferromagnetic nanoparticles. *Nat. Nanotechnol.* **2007**, *2*, 577–583. [[CrossRef](#)]

**Disclaimer/Publisher’s Note:** The statements, opinions and data contained in all publications are solely those of the individual author(s) and contributor(s) and not of MDPI and/or the editor(s). MDPI and/or the editor(s) disclaim responsibility for any injury to people or property resulting from any ideas, methods, instructions or products referred to in the content.